NASA/CR-2001-211036
ICASE Report No. 2001-21

Computation of Nonlinear Backscattering Using a High-order Numerical Method

G. Fibich and B. Ilan
Tel Aviv University, Tel Aviv, Israel

S. Tsynkov
Tel Aviv University, Tel Aviv, Israel and
North Carolina State University, Raleigh, North Carolina

ICASE
NASA Langley Research Center
Hampton, Virginia

Operated by Universities Space Research Association

National Aeronautics and
Space Administration

Langley Research Center
Hampton, Virginia 23681-2199

Prepared for Langley Research Center
under Contract NAS1-97046

July 2001

COMPUTATION OF NONLINEAR BACKSCATTERING USING A HIGH-ORDER NUMERICAL METHOD*

G. FIBICH†‡, B. ILAN†§, AND S. TSYNKOV†¶

Abstract. The nonlinear Schrödinger equation (NLS) is the standard model for propagation of intense laser beams in Kerr media. The NLS is derived from the nonlinear Helmholtz equation (NLH) by employing the paraxial approximation and neglecting the backscattered waves. In this study we use a fourth-order finite-difference method supplemented by special two-way artificial boundary conditions (ABCs) to solve the NLH as a boundary value problem. Our numerical methodology allows for a direct comparison of the NLH and NLS models and for an accurate quantitative assessment of the backscattered signal.

Key words. Kerr medium, wave propagation, self focusing, fourth-order method, two-way ABCs

Subject classification. Applied and Numerical Mathematics

1. Introduction. The propagation of intense laser beams (time-harmonic electromagnetic waves) in a bulk Kerr medium is usually modeled by the critical nonlinear Schrödinger equation (NLS) for the electric field amplitude. Since light rays bend toward areas with higher index of refraction, the nonlinear dependence of the index of refraction on beam intensity has a *self-focusing* effect, whereby a sufficiently intense laser beam becomes narrower as it propagates. In particular, the NLS model predicts that when the input beam power (L^2 norm) exceeds a given critical threshold N_c, then the beam can collapse to a point at a finite propagation distance. For more information of self-focusing, see e.g., [6, 9].

As the beam propagates it induces changes in the optical properties of the medium. As a result, part of the incoming wave is reflected back, a phenomenon referred to as *backscattering*. Very little is actually known on backscattering in nonlinear self-focusing, except for the general belief that it is "small." Since, however, small-magnitude mechanisms can have a large effect in self-focusing [6], there is a need to accurately quantify the magnitude of backscattering and study how this phenomenon may affect the beam propagation. Another application which could greatly benefit from better understanding of backscattering is remote sensing of the atmosphere [12], where the measured signal is exactly the backscattered wave.

The backscattered wave is neglected in the NLS model which only describes the forward-propagating wave. Calculation of backscattering requires, therefore, going back to the nonlinear Helmholtz equation (NLH), from which the NLS is derived. The NLS is an evolution equation with the spatial coordinate in the direction of propagation playing the role of "time." Therefore, the correct mathematical formulation for the NLS is the Cauchy (initial value) problem and as such, solving it numerically is a relatively straightforward computational procedure. In contradistinction to that, the NLH is elliptic in its nature, and a special multidimensional boundary value problem needs to be formulated and solved for this equation, which is a much harder task from the standpoint of computing. The first numerical simulations based on solving a

*This research was supported by the National Aeronautics and Space Administration under NASA Contract No. NAS1–97046 while the third author was in residence at ICASE, NASA Langley Research Center, Hampton, VA 23681–2199, USA.

†School of Mathematical Sciences, Tel Aviv University, Ramat Aviv, Tel Aviv 69978, Israel.

‡E-mail: fibich@math.tau.ac.il, URL: www.math.tau.ac.il/∼fibich. Work supported by grant 97-00127 from the United States–Israel Binational Science Foundation (BSF), Jerusalem, Israel.

§E-mail: bazooka@math.tau.ac.il, URL: www.math.tau.ac.il/∼bazooka.

¶Department of Mathematics, North Carolina State University, Box 8205, Raleigh, NC 27695, USA. Phone: (1-919)515-1877, Fax: (1-919)515-3798. E-mail: tsynkov@math.ncsu.edu, URL: www.math.ncsu.edu/∼stsynkov.

boundary value problem for the NLH were recently performed in [7] using an advanced fourth-order method. In that study, the design fourth-order convergence rate of the method was corroborated experimentally on a model linear problem. Subsequently, a series of the grid convergence tests were conducted in the nonlinear regime. In the current paper we go beyond grid-convergence arguments and show that the asymptotic limit of the NLH solutions obtained in the simulations is the corresponding NLS solution. This comparison provides strong support that the calculated NLH solution is indeed the physical one. In Section 2.3 we obtain an asymptotic estimate of the magnitude of backscattering and subsequently show in Section 4 that it agrees with the calculated values.

When the initial datum is sufficiently large the NLS solution develops singularities at a finite propagation distance (see Section 2.5). Since, however, physical quantities do not become infinite, a natural question is whether the corresponding solution of the NLH exists globally. This fundamental question has been open for many years. There have been indications, though, that solutions to the NLH exist even when the corresponding NLS solutions become singular, based on both numerical solution of "modified" NLH equations [1,2,4] and on asymptotic analysis [5], but these studies did not take into account backscattering effects. Therefore, our long-term goal is to solve the NLH for those incoming signals that lead to blowup in the NLS model. In the current study, however, we concentrate on the more attainable goal of better understanding (in terms of both analysis and numerical simulations) the regime when the corresponding solution of the NLS does not blow up. Our hope is that this understanding will eventually allow to solve the NLH for "any" incoming signal.

2. Mathematical Models.

2.1. The Nonlinear Helmholtz Equation. A typical experimental setup (both physical and numerical) for the propagation of waves in Kerr media is shown in Figure 2.1. An incoming laser beam with known characteristics impinges normally on the planar interface $z = 0$ between the linear and the nonlinear media. The electric field $E = E(x_1, \ldots, x_{D-1}, z)$ in $\mathbb{R}^D$ is governed by the nonlinear Helmholtz equation

$$(\partial_{zz} + \Delta_\perp)E + k^2 E = 0, \quad k^2 = k_0^2(1 + \epsilon|E|^{2\sigma}), \quad (x_1, \ldots, x_{D-1}) \in \mathbb{R}^{D-1}, \quad z \geq 0, \tag{2.1}$$

where k_0 is the wavenumber, $\epsilon = 4\epsilon_0 c n_2$, n_2 is the Kerr coefficient, and $\Delta_\perp = \partial_{x_1 x_1} + \ldots + \partial_{x_{D-1} x_{D-1}}$ is the transverse Laplacian (the diffraction term), see, e.g., [3,8]. For simplicity we consider from now on the cylindrically-symmetric case where $E = E(r, z)$ and $r = \sqrt{x_1^2 + \ldots + x_{D-1}^2}$.

The nonlinear medium occupies the semi-space $z \geq 0$ (see Figure 2.1). Consequently, the NLH (2.1) has to be supplemented by boundary conditions at $z = 0$ and $z \longrightarrow +\infty$. We require that as $z \longrightarrow +\infty$, E has no left-traveling components and that the propagation is diffraction-dominated with the field amplitude decaying to zero, i.e., $\lim\limits_{z\to\infty} \max\limits_{0\leq r<\infty} |E(r, z)| = 0$, which also means $\lim\limits_{z\to+\infty} k^2 = k_0^2$. In other words, at large z's the solution should be a linear superposition of right-traveling waves. Since the actual numerical simulation is carried out on a truncated domain $0 \leq z \leq z_{\max}$ (Figure 2.1), the desired behavior of the solution as $z \longrightarrow +\infty$ has to be captured by a far-field artificial boundary condition (ABC) at the artificial boundary $z = z_{\max}$. This boundary condition should guarantee a reflectionless propagation of all the waves traveling toward $z = +\infty$. Often, boundary conditions designed to ensure the transparency of the outer boundary to the outgoing waves are called *radiation boundary conditions* [10].

The situation is more complicated at the interface $z = 0$, where the total field $E(r, 0)$ is composed of a given incoming (right-traveling) component $E_{\text{inc}}(r, 0)$ and an unknown backscattered (left-traveling)

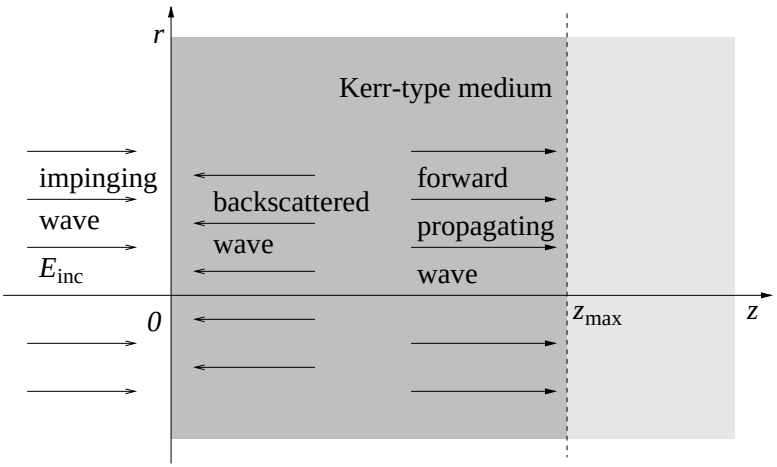

FIG. 2.1. *Schematic of propagation of waves in Kerr media.*

component $E_{\text{scat}}(r,0)$, i.e.,

$$E(r,0) = E_{\text{inc}}(r,0) + E_{\text{scat}}(r,0) \ .$$

As such, the boundary condition at $z = 0$ has to guarantee the reflectionless propagation of any left-traveling wave through the interface and at the same time be able to correctly prescribe the incoming signal. Implementation of such *two-way ABC* was done in [7].

Finally, we assume symmetry at $r = 0$ and vanishing of the electric field as $r \longrightarrow +\infty$. In practice, we truncate the domain at some large but finite $r_{\max}$ and require that $E(r_{\max}, z) = 0$. The justification for the use of this approach to treat the "lateral" boundaries can be found in [10] and the bibliography there.

Let us also note that in this study we do not take into account the effect of discontinuity in the index of refraction across the interface $z = 0$. Thus, we assume that $E_{\text{inc}}(r,0)$ is the incoming wave after it has already passed through the interface (i.e., at $z = 0+$). We also assume that left-traveling (i.e., backscattered) waves are not reflected by the interface $z = 0$ back into the domain $z \geq 0$. One can expect the latter effect to be small; it will be investigated in a future study.

2.2. Paraxial Approximation and the Nonlinear Schrödinger Equation. Let r_0 be the initial width of the impinging beam. We first introduce the dimensionless quantities $\tilde{r}$, $\tilde{z}$, and ψ as

$$\tilde{r} = \frac{r}{r_0} \ , \quad \tilde{z} = \frac{z}{2L_{DF}} \ , \quad E = e^{ik_0 z}(\epsilon r_0^2 k_0^2)^{-1/2\sigma}\psi(r,z) \ , \tag{2.2}$$

where $L_{DF} = k_0 r_0^2$ is the *diffraction length*. Then, by dropping the tildes we obtain

$$i\psi_z + \Delta_\perp \psi + |\psi|^{2\sigma}\psi = -4f^2\psi_{zz} \ , \tag{2.3}$$

where $f = 1/r_0 k_0 \ll 1$ is the *nonparaxiality parameter*.

The standard derivation of the NLS is based on the assumption that the envelope ψ is slowly varying. In that case, one can neglect the term on the right-hand side of (2.3) [i.e., apply the *paraxial approximation*] and obtain the nonlinear Schrödinger equation

$$i\psi_z + \Delta_\perp \psi + |\psi|^{2\sigma}\psi = 0 \ . \tag{2.4}$$

The NLS (2.4) is supplemented by the initial condition at $z = 0$

$$\psi(r,0) = (\epsilon r_0^2 k_0^2)^{1/2\sigma} E_{\text{inc}}(r,0) \ .$$

Subsequently, it needs to be integrated by a "time"-marching algorithm, where the direction of propagation z plays the role of time. We reemphasize that *backscattering effects are not taken into account by the NLS (2.4).* Indeed, once (2.4) is solved, the overall solution, according to (2.2), is the slowly varying amplitude ψ times the forward propagating oscillatory component $e^{ik_0 z}$.

2.3. Preliminary Analysis of Backscattering. To the best of our knowledge, no accurate quantitative analysis of backscattering in nonlinear self-focusing has ever been performed, although there is a general belief that the magnitude of the backscattered signal is small. In this section we present a preliminary asymptotic study of backscattering. To do that, we consider a more general ansatz for E than (2.2) which is composed of both forward-propagating and backward-propagating waves, i.e.,

$$E = (\epsilon r_0^2 k_0^2)^{-1/2\sigma} \left[A(r,z) e^{ik_0 z} + B(r,z) e^{-ik_0 z} \right] , \tag{2.5}$$

where A and B are slowly-varying envelopes. Substitution in the NLH (2.1) yields

$$e^{ik_0 z} \left[A_{zz} + 2ik_0 A_z + \Delta_\perp A + |A + e^{-2ik_0 z} B|^{2\sigma} A \right] + e^{-ik_0 z} \left[B_{zz} + 2ik_0 B_z + \Delta_\perp B + |A + e^{-2ik_0 z} B|^{2\sigma} B \right] = 0 .$$

Changing to the nondimensional variables (2.2) gives (after dropping the tildes)

$$e^{i(4/f^2)z} \left[f^2 A_{zz} + iA_z + \Delta_\perp A + |A + e^{-i(4/f^2)z} B|^{2\sigma} A \right] + \left[f^2 B_{zz} + iB_z + \Delta_\perp B + |A + e^{-i(4/f^2)z} B|^{2\sigma} B \right] = 0 .$$

Let us average the last equation over one fast oscillation. For example, using Taylor expansion, we obtain

$$\frac{2}{\pi f^2} \int_{z-\pi f^2/4}^{z+\pi f^2/4} B(\zeta)\, d\zeta = \frac{2}{\pi f^2} \int_{z-\pi f^2/4}^{z+\pi f^2/4} [B(z) + (\zeta - z) B_z(z) + \ldots]\, d\zeta = B(z)(1 + O(f^2)) .$$

Similarly,

$$\begin{aligned} \frac{2}{\pi f^2} \int_{z-\pi f^2/4}^{z+\pi f^2/4} e^{i(4/f^2)z} A(\zeta)\, d\zeta &= \frac{2}{\pi f^2} \int_{z-\pi f^2/4}^{z+\pi f^2/4} e^{i(4/f^2)z} [A(z) + (\zeta - z) A_z(z) + \ldots]\, d\zeta \\ &= \frac{f^2}{4i} A_z e^{i(4/f^2)z} + O(f^4) . \end{aligned}$$

Consequently, we obtain the following equation for the backscattered wave

$$f^2 B_{zz} + iB_z + \Delta_\perp B + |A + e^{-i(4/f^2)z} B|^{2\sigma} B = f^2 F , \qquad B(z)\Big|_{z=\infty} = 0 , \tag{2.6}$$

where

$$F = \frac{1}{4i} e^{i(4/f^2)z} \left[f^2 A_{zz} + iA_z + \Delta_\perp A + |A + e^{-i(4/f^2)z} B|^{2\sigma} A \right]_z .$$

Let us now employ the common assumption that backscattering is small, i.e., $B \ll A$. Since $f \ll 1$, equation (2.6) for B can be approximated with the linear Schrödinger equation

$$iB_z + \Delta_\perp B + |A|^{2\sigma} B = f^2 F, \qquad B(z)\Big|_{z=\infty} = 0 ,$$

where

$$F = \frac{1}{4i} e^{i(4/f^2)z} \left[iA_z + \Delta_\perp A + |A|^{2\sigma} A \right]_z .$$

Since the solution of

$$iB_z + \Delta_\perp B + |A|^{2\sigma} B = 0 \ , \qquad B(z)\Big|_{z=\infty} = 0 \ ,$$

is $B \equiv 0$, the above analysis suggests that

$$B/A = O(f^2) \ . \tag{2.7}$$

If the quadratic scaling law (2.7) can be confirmed independently, then it will provide a convincing justification for the assumption that backscattering is indeed small. Hence, in our simulations we expect to see that

$$\frac{(\epsilon r_0^2 k_0^2)^{1/2\sigma} |E| - |A|}{|A|} = O(f^2). \tag{2.8}$$

The numerical results of Section 4 do corroborate these expectations.

The above analysis also shows that

$$|E| = \left(\epsilon r_0^2 k_0^2\right)^{-1/2\sigma} |A| \left| 1 + \frac{B}{A} e^{-2ik_0 z} \right| \ .$$

Therefore, the amplitude of the NLH solution may have $O(f^2)$ ripples with the wavelength π/k_0 due to backscattering on top of the slowly varying amplitude of the forward-propagating wave. NLH simulations suggesting that this indeed may be the case have been reported in [7] (see also Figure 4.2 in Section 4). It is not clear, however, to what extent the ripples observed in [7] are a numerical artifact due to placing the far-field artificial boundary too close to the nonlinear self-focusing zone. Numerical study conducted in [7] did, in fact, involve the analysis of how the location of the far-field artificial boundary affects the solution; placing this boundary further and further away caused the reduction in the ripples' magnitude but never allowed to eliminate them completely. This may still imply, though, that the boundary was not "sufficiently far" away. Therefore, no definite conclusion as to the presence of the $O(f^2)$ ripples in the NLH solutions can be made at this time and this question requires a subsequent thorough study.

2.4. Nonparaxiality and backscattering. The traditional way of introducing the paraxial approximation is reported in Section 2.2, where the right-hand side of equation (2.3) is omitted and the NLS is derived. The more careful analysis of Section 2.3 shows, however, that *two approximations* are, in fact, being made when the NLH is approximated with the NLS: Neglecting A_{zz} (the paraxial approximation in the narrow sense, i.e., as it applies to the forward-propagating waves) and neglecting B (backscattering). We recall that previous studies [4, 5] suggested that nonparaxiality of the right-traveling waves (i.e., A_{zz} in the sense of Section 2.3) arrests the collapse of the NLS solutions, but these studies did not take into account backscattering effects. Having said that, we still note that the separation into nonparaxial and backscattering effects, which is based on the ansatz (2.5), is somewhat artificial, since the problem in nonlinear. Therefore, when we compare the NLH and NLS solutions, it is not precisely clear which part of the difference comes from nonparaxial effects for the right-traveling waves, and which one from backscattering. *A notable exception is, however, at $z = 0$, where the difference between NLH and NLS solutions is solely due to backscattering.*

2.5. Critical NLS. It is well known that solutions of the NLS (2.4) can become singular when either $\sigma(D-1) > 2$, the *supercritical* NLS, or when $\sigma(D-1) = 2$, the *critical* NLS (D is the space dimension). However, whereas in supercritical collapse nonlinearity dominates over diffraction near the singularity, in the critical collapse nonlinearity and diffraction are almost balanced near the singularity. Consequently, the

singularity formation is highly sensitive to small perturbations in the critical case, but much less so is the supercritical case.

The physical case that corresponds to the propagation of laser beams in bulk Kerr media is the critical one, as $D = 3$ and $\sigma = 1$. However, in order to reduce the complexity of the computations, below we consider the critical case $D = 2$ and $\sigma = 2$. Thus, the NLH for $E = E(r, z)$ and the NLS for $\psi = \psi(r, z)$, which are solved numerically in this study are

$$E_{zz} + E_{rr} + k_0^2(1 + \epsilon|E|^4)E = 0 \ , \tag{2.9}$$

and

$$i\psi_z + \psi_{rr} + |\psi|^4\psi = 0 \ , \tag{2.10}$$

respectively.

3. Numerical Methods. The NLH (2.9) is solved using fourth-order finite differences. The choice of a higher-order method is motivated primarily by the necessity to resolve a small-scale phenomenon (backscattering) at the background of the forward propagating waves. The NLS (2.10) is also solved by a fourth-order scheme; it is natural to expect that this will leave less room for potential purely numerical discrepancies between the two techniques and as such, will allow for a more accurate comparison. Besides, it is generally known that higher-order methods provide for a better resolution of waves.

3.1. Numerical Integration of the NLH. Our numerical method for solving the NLH is delineated in [7]; here we only outline its key elements. We use a conventional fourth-order central-difference discretization of the Laplacian; in so doing the stencil is five-node wide in both r and z directions. As the equation is nonlinear, we implement a nested iteration scheme. On the outer loop, we freeze the nonlinearity, i.e., consider the coefficient k^2 of (2.1) as a given function of r and z, which is actually obtained by taking $|E|^4$ from the previous iteration. This way we arrive at a linear equation with variable coefficients. The latter is also solved by iterations on the inner loop of the nested scheme. Here, we leave the entire varying part of the equation, which is proportional to ϵ, on the lower level, and on the upper level need to invert only the constant-coefficient linear Helmholtz operator $\Delta + k_0^2\boldsymbol{I}$. Formally, our iteration scheme resembles the fixed-point approach, however, no rigorous convergence theory is available yet, and the convergence has to be assessed experimentally. The advantage of using these nested iterations is that first, the method eventually reduces to the repeated solution of one and the same linear constant coefficient equation driven by different source terms. As explained below, this can be done efficiently on the discrete level. Second, the radiation boundary conditions and the two-way ABCs are most convenient to set on the upper time level of the iteration scheme already for the linear constant-coefficient operator.

To solve the linear-constant coefficient Helmholtz equation (discrete counterpart of $\Delta E + k_0^2 E = g$, where g is the right-hand side generated on the previous iteration) we first separate the variables by implementing the discrete Fourier transform in the transverse direction r; the boundary conditions are symmetry at $r = 0$ and zero Dirichlet at $r = r_{\max}$. This yields a collection of fourth-order one-dimensional finite-difference equations parameterized by the dual Fourier variable; each of the latter needs to be solved independently. The two-way and radiation ABCs at $z = 0$ and $z = z_{\max}$, respectively, are set in the Fourier space as well, i.e., separately for each of the aforementioned one-dimensional equations. This is done by first identifying the linearly-independent eigen-modes for the homogeneous version of each one-dimensional equation. It is important to note that even though the original differential equation is of the second order, we are

using its fourth-order approximation and as such, each homogeneous discrete one-dimensional equation has four linearly independent solutions. One pair of the latter approximates the genuine modes of the differential equation, those may be either traveling or evanescent waves depending on the value of the dual Fourier variable. The other pair is a pure numerical artifact, these waves are always evanescent, but their presence implies that every discrete equation requires two more boundary conditions compared to the original differential equation. The radiation boundary conditions are constructed by requiring that on the left boundary $z = 0$ only the left-traveling and/or left-decaying (evanescent) waves be present in the solution, and on the right boundary $z = z_{\max}$ only the right-traveling and/or right-evanescent waves be present in the solution. The selection is rendered by the so-called one-way discrete Helmholtz equations, which are the linear homogeneous relations that define the span of all appropriate modes for each boundary. The two-way ABC that also prescribes the incoming signal at $z = 0$ is constructed on the basis of the corresponding radiation boundary condition by substituting the right-traveling incoming wave into the one-way-to-the-left Helmholtz equation and as such creating the inhomogeneity of a particular form, see [7]. Simple considerations based on the linear superposition principle and uniqueness guarantee that the resulting nonhomogeneous relation will correctly specify the incoming signal at $z = 0$ and still ensure the reflectionless propagation of all the outgoing (i.e., left-traveling) waves through $z = 0$ toward $z = -\infty$.

As concerns the computational complexity of the resulting algorithm, if we introduce the grid dimensions N_r and N_z, then the cost of both the direct and inverse FFT will be $O(N_z N_r \ln N_r)$. The cost of solving each of the N_r one-dimensional systems will be linear with respect to N_z. Indeed, in the course of iterations each of these systems needs to be solved many times for different right-hand sides. Consequently, the sparse LU decomposition can be performed only once ahead of time, and the cost of each backward substitution is linear. Altogether, the complexity of each iteration is still $O(N_z N_r \ln N_r)$.

3.2. Numerical Integration of the NLS. The NLS (2.10) is discretized in the r direction using standard fourth-order central differences. It is integrated in z with a four-stage Runge-Kutta method starting with the initial data $E_{\text{inc}}(r, 0)$. The boundary condition at the remote lateral boundary $r = r_{\max}$ is zero Dirichlet, as in the case of the NLH.

4. Computational Results. In accordance with the discussion of Section 2 we have designed a set of numerical experiments aimed at achieving two objectives: (I) Validate the computational algorithm of [7] for solving the NLH through a comparison with numerical simulations of the NLS model, and (II) corroborate that backscattering effects captured by the NLH model scale quadratically with the nonparaxiality parameter f, as suggested by the analysis of Sections 2.3–2.4. Regarding the first objective, let us note that previously we have tested the numerical algorithm of [7] in the nonlinear regime using grid convergence, but never compared it with any other algorithm for computing the propagation of waves in Kerr media. As concerns the second objective, it amounts to the accurate numerical computation of backscattering in nonlinear self-focusing, and we are currently unaware of any previous technique with similar capabilities.

To be able to conduct an accurate comparison of the numerical predictions obtained with the NLH and NLS models (equations (2.9) and (2.10), respectively), we have chosen a regime with the input power below critical, for which the solution of the NLS does not develop singularities. We take $k_0 = 8$ and $\epsilon = 0.04$, which corresponds to 74% of the critical power N_c, see [7, 11]. The incoming beam profile is $E_{\text{inc}}(r, 0) = e^{-(r/r_0)^2}$, such that the beam width r_0 is much less than $r_{\max}$. To allow for the variation of the nonparaxiality parameter $f = 1/k_0 r_0$, we vary the beam width r_0 while keeping the wavenumber k_0 and the quantity $k_0\sqrt{\epsilon}$ that controls the fractional critical power unchanged.

In Figure 4.1 we show the on-axis amplitude profiles for the NLH and NLS numerical solutions;

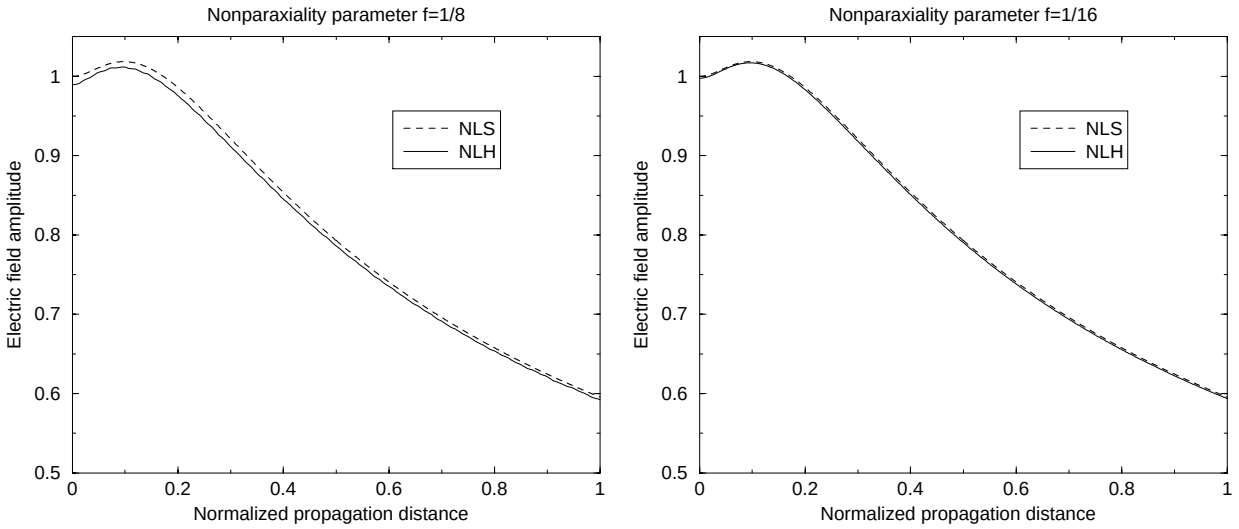

FIG. 4.1. *On-axis amplitudes of the solutions to NLH:* $|E(0,z)|$, *and NLS:* $(\epsilon r_0^2 k_0^2)^{-1/4}|\psi(0,z)|$, *plotted vs.* $z/2L_{DF}$.

Figure 4.1(left) corresponds to $f = 1/8$, and Figure 4.1(right) corresponds to $f = 1/16$. We plot the values of the computed solution on the axis of symmetry $r = 0$ because this is the most interesting location in the domain where the genuinely nonlinear phenomena take place. A clear manifestation of nonlinear self-focusing is the "bump," or peak, on the solution curves in Figure 4.1, whose value is *higher* than that of the incoming wave $E_{\rm inc}(0,0)$.

It is easy to see that for both $f = 1/8$ and $f = 1/16$ the NLH and NLS curves in Figure 4.1 are close to one another. As the NLS is a well-established model that has regular solutions for subcritical initial powers, we conclude that our numerical algorithm for solving the NLH [7] [that starts the iteration process with the initial guess $E \equiv 0$] indeed converges to the correct solution.

We also notice that the discrepancy between the NLH and NLS curves on Figure 4.1(left) is larger than that on Figure 4.1(right). This behavior is expected according to the analysis of Section 2.3, because the discrepancy between the two curves is due to nonparaxiality and backscattering. In particular, these simulations suggest that the NLS is indeed the asymptotic limit of the NLH as $f \longrightarrow 0$. Perhaps the most apparent manifestation of the presence of backscattering in the solution of the NLH is that the computed value of the total electric field at $z = 0$ *differs* from that of the incoming wave, as one can clearly see in Figure 4.2 where we zoom in on the two curves obtained for $f = 1/8$. The small ripples in the NLH solution may also be evidence of backscattering (see Section 2.3).

Next, we quantify the backscattering effect by computing a series of solution pairs (NLS and NLH) for additional values of f. In Figure 4.3(left) we show by asterisks on the log-log scale the quantity

$$\left|\left(\epsilon k_0^2 r_0^2\right)^{1/4} E(0,0) - \psi(0,0)\right| \equiv \left|\left(\epsilon k_0^2 r_0^2\right)^{1/4} E(0,0) - A(0,0)\right| \tag{4.1}$$

(cf. formula (2.8)), where E is the computed solution of the NLH and ψ is the solution to the NLS that satisfies the initial condition $\psi(0,0) = 1$, for $f = 1/16, 1/12, 1/10,$ and $1/8$. The solid line on Figure 4.3(left) that fits closely the computed data is $0.75 \cdot f^{2.05}$. This essentially corroborates that the magnitude of backscattering indeed scales quadratically with the nonparaxiality parameter f, as predicted in Section 2.3 and further discussed in Section 2.4.

Let us also note that to evaluate the quantity (4.1) we do not really need to solve the NLS, because the

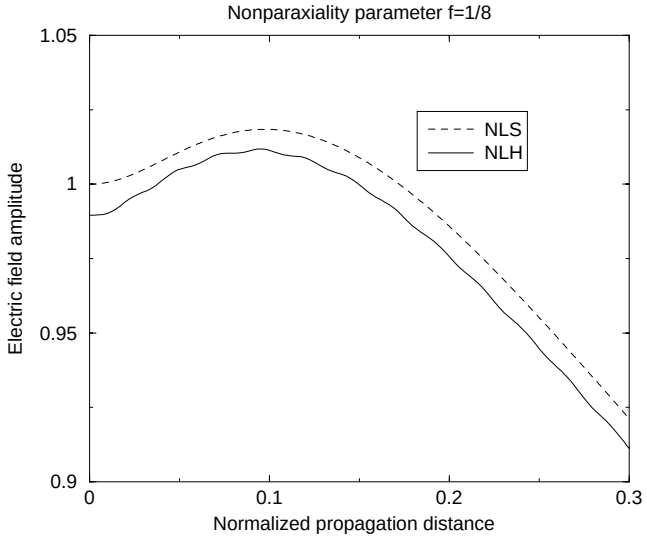

FIG. 4.2. *Zoom-in on Figure 4.1(left) in the area of the nonlinear self-focusing peak.*

initial profile at $z = 0$ is given. To compare the actual computed solutions of the NLH and NLS, we plot on Figure 4.3(right) the quantity

$$\left| \left(\epsilon k_0^2 r_0^2\right)^{1/4} |E(0,z)| - |\psi(0,z)| \right| \tag{4.2}$$

for $f = 1/8$ and $f = 1/16$ (same values as on Figure 4.1) as a function of the normalized propagation distance for $z \geq 0$. Although the curves on Figure 4.3(right) are oscillatory, we still see that that the difference between the solutions of the NLH and NLS decreases for all z with the decrease of f.

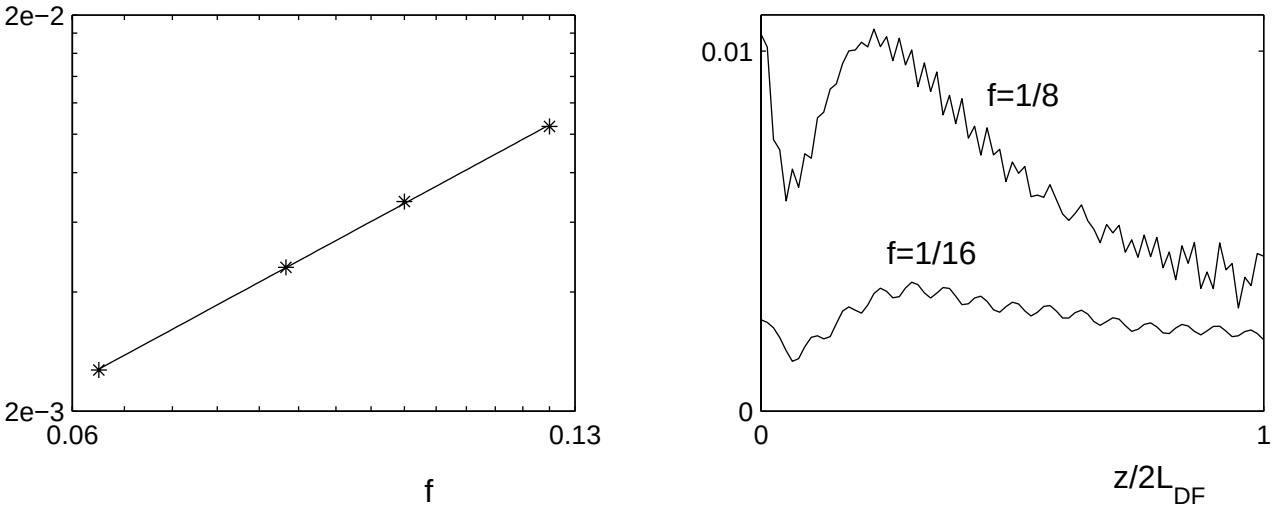

FIG. 4.3. *Left: The quantity given by formula (4.1) as a function of f compared on the log-log scale with the approximation $0.75 \cdot f^{2.05}$ (solid line). Right: The difference (4.2) between the two solutions as a function of $z/2L_{DF}$ for $f = 1/8$ and $f = 1/16$.*

5. Conclusions. We have compared numerically the solutions to the nonlinear Schrödinger equation and nonlinear Helmholtz equation, both of which model the propagation of time-harmonic electromagnetic

waves in Kerr media. The NLH was solved using a new fourth-order method supplemented by the two-way artificial boundary conditions that guarantee the proper behavior of the waves as they enter and leave the computational domain. As the NLS is considered an established model, the agreement of the NLH and NLS simulations provides a good justification that the NLH algorithm indeed converges to the correct physical solution. On the other hand, the NLH is a more comprehensive model that, unlike the NLS, takes into account the phenomenon of nonlinear backscattering. As such, we attribute the small discrepancies that do exist between the NLH and NLS solution to nonparaxial and backscattering effects. By analyzing several computational variants that correspond to different values of the nonparaxiality parameter f we have been able to corroborate that the magnitude of the backscattered wave indeed scales quadratically with this parameter, according to the theoretical predictions. To the best of our knowledge, this is the first study ever that allows for an accurate quantitative estimation of backscattering in nonlinear self-focusing.

Acknowledgment. G. Fibich would like to acknowledge useful discussions with G. Papanicolaou.

REFERENCES

[1] N. Akhmediev, A. Ankiewicz, and J. Soto-Crespo, *Does the nonlinear Schrödinger equation correctly describe beam propagation?*, Opt. Lett., 18 (1993), pp. 411–413.

[2] N. Akhmediev and J. Soto-Crespo, *Generation of a train of three-dimensional optical solitons in a self-focusing medium*, Phys. Rev. A, 47 (1993), pp. 1358–1364.

[3] R. Boyd, *Nonlinear Optics*, Academic Press, Boston, 1992.

[4] M. Feit and J. Fleck, *Beam nonparaxiality, filament formation, and beam breakup in the self-focusing of optical beams*, J. Opt. Soc. Am. B, 5 (1988), pp. 633–640.

[5] G. Fibich, *Small beam nonparaxiality arrests self-focusing of optical beams*, Phys. Rev. Lett., 76 (1996), pp. 4356–4359.

[6] G. Fibich and G. Papanicolaou, *Self-focusing in the perturbed and unperturbed nonlinear Schrödinger equation in critical dimension*, SIAM J. Applied Math., 60 (1999), pp. 183–240.

[7] G. Fibich and S. Tsynkov, *High-order two-way artificial boundary conditions for nonlinear wave propagation with backscattering*, J. Comput. Phys., 171 (2001), pp. 1–46.

[8] A. Newell and J. Moloney, *Nonlinear optics*, Addison-Wesley, Redwood City, Calif., 1992.

[9] C. Sulem and P. Sulem, *The nonlinear Schrödinger equation*, Springer, New-York, 1999.

[10] S. Tsynkov, *Numerical solution of problems on unbounded domains. A review*, Appl. Numer. Math., 27 (1998), pp. 465–532.

[11] M. Weinstein, *Nonlinear Schrödinger equations and sharp interpolation estimates*, Comm. Math. Phys., 87 (1983), pp. 567–576.

[12] L. Wöste, C. Wedekind, H. Wille, P. Rairoux, B. Stein, S. Nikolov, C. Werner, S. Niedermeier, F. Ronnenberger, H. Schillinger, and R. Sauerbrey, *Femtosecond atmospheric lamp*, Laser und Optoelektronik, 29 (1997), pp. 51–53.